Clim. Past Discuss., 11, 5269–5306, 2015
www.clim-past-discuss.net/11/5269/2015/
doi:10.5194/cpd-11-5269-2015

Climate of the Past Discussions
Open Access
EGU

Marine sediment records as indicator for the changes in Holocene Saharan landscape: simulating the dust cycle

S. Egerer[1,2], M. Claussen[1,3], C. Reick[1], and T. Stanelle[4]

[1]Max Planck Institute for Meteorology, Bundesstraße 53, 20146 Hamburg, Germany
[2]International Max Planck Research School on Earth System Modelling, Bundesstraße 53, 20146 Hamburg, Germany
[3]Center for Earth System Research and Sustainability, Universität Hamburg, Bundesstraße 53, 20146 Hamburg, Germany
[4]Center for Climate System Modeling, ETH Zurich, Universitätstraße 16, 8092 Zurich, Switzerland

Received: 13 October 2015 – Accepted: 27 October 2015 – Published: 10 November 2015

Correspondence to: S. Egerer (sabine.egerer@mpimet.mpg.de)

Published by Copernicus Publications on behalf of the European Geosciences Union.

Abstract

Marine sediment records reveal an abrupt and strong increase in dust deposition in the North Atlantic at the end of the African Humid Period about 5500 years ago. The change in dust flux has been attributed to varying Saharan land surface cover. Alternatively, variability in climate and ocean conditions, for example changes in sea surface temperature, have been proposed to explain the enhanced dust deposition. Here we demonstrate for the first time the direct link between dust accumulation in marine cores and Saharan land surface. We simulate the mid-Holocene (6 ka BP) and pre-industrial (1850 AD) dust cycle as a function of Saharan land surface cover and atmosphere–ocean conditions using the coupled atmosphere-aerosol model ECHAM6-HAM2.1. Mid-Holocene surface characteristics, including vegetation cover and lake surface area, are derived from proxy data and simulations. In agreement with data from marine sediment cores, our simulations show that mid-Holocene dust deposition fluxes in the North Atlantic were two to three times lower compared with pre-industrial fluxes. We identify Saharan land surface characteristics to be the main control on dust transport from North Africa to the North Atlantic. We conclude that the variation in dust accumulation in marine cores is likely related to a transition of the Saharan landscape during the Holocene and not due to changes in atmospheric or ocean conditions.

1 Introduction

The transition from the "green" Sahara of the early to mid-Holocene, about 9 to 6 ka BP, to today's hyperarid conditions was triggered by a steady shift in orbital forcing. Thereby, the Northern Hemisphere received about 4.2 % more summer insolation during the early to mid-Holocene compared to present times (Berger, 1978) causing a higher temperature gradient between the North African subcontinent and the Eastern Atlantic Ocean. This led to a strengthening of the West African summer monsoon and a consequent northward shift of the West African rain belt (Kutzbach, 1981). A wet

CPD
11, 5269–5306, 2015

climate supported the establishment of permanent vegetation cover and lakes in the area of today's hyperarid Sahara (Kutzbach and Street-Perrott, 1985; Jolly et al., 1998; Kohfeld and Harrison, 2000). Pollen records indicate a considerable expansion of vegetation in North Africa north of 15° N at that time (Prentice et al., 2000) with steppe, savanna and temperate xerophytic woods and shrubs extending up to 23° N (Jolly et al., 1998). Lakes and wetlands were widespread up to 30° N and covered about 7.6 % of North Africa (Hoelzmann et al., 1998; Jolly et al., 1998; Kröpelin et al., 2008; Street-Perrott et al., 1989). The largest water body was lake Mega-Chad with an area of at least 350 000 km^2 presumably (Schuster et al., 2005).

Marine sediment cores along the northwest African margin reveal an abrupt and strong increase in dust accumulation in the North Atlantic of about 50 % (DeMenocal et al., 2000) up to a factor of 5 (McGee et al., 2013) some 5500 years ago. The change in dust flux has been attributed to varying Saharan vegetation cover predicted by Brovkin et al. (1998) and Claussen et al. (1999) or was related to a change in lake surface area (Armitage et al., 2015; Cockerton et al., 2014). Alternatively, variability in climate or ocean circulation, for example sea surface temperature deviations, could explain the enhanced dust accumulation (Adkins et al., 2006). However, until now there has been no modeling study that explicitly simulated the mid-Holocene dust cycle to assure the link between Saharan land surface cover and North Atlantic dust deposits at the particular location of the marine cores.

Two modeling studies of the dust cycle using general circulation models (GCMs) have covered the mid-Holocene era. Albani et al. (2014) performed two simulations of a 6 ka BP and a pre-industrial time slice using the Community Earth System Model (CESM) including a Bulk Aerosol Model (CAM4-BAM). Vegetation was set to pre-industrial conditions according to PMIP/CMIP prescriptions for both time slices. The soil erodibility was then scaled for each grid cell based on vegetation cover, which was obtained offline by BIOME4 simulations. The other GCM study was published by Sudarchikova et al. (2015) using the ECHAM5-HAM model. They performed simulations of the global dust cycle for several time slices including pre-industrial and mid-

CPD
11, 5269–5306, 2015

Holocene. Paleoclimatic vegetation was simulated with the dynamic vegetation model LPJ-GUESS. They obtained a similar fractional vegetation cover distribution in North Africa for mid-Holocene and pre-industrial, which is at variance with reconstructions. Both models underestimate the extent of mid-Holocene vegetation cover suggested by pollen data (Hoelzmann et al., 1998; Jolly et al., 1998). As sparse or non-vegetated areas are potential dust sources, dust emission from North Africa was thus overestimated for the mid-Holocene. Additionally, the extent of paleolakes was not taken into account in either study, despite the fact that areas covered by lakes loose their potential as a dust source. Accordingly, marine sediment records along the West African margin (McGee et al., 2013; DeMenocal et al., 2000) indicate a lower global dust accumulation rate than suggested in the modeling studies.

To overcome the shortcomings of previous simulation studies on the mid-Holocene dust cycle, we account for a realistic land surface cover prescribing mid-Holocene vegetation conditions in North Africa based on reconstructions of Hoelzmann et al. (1998) and specifying the distribution of paleolakes from simulations (Tegen et al., 2002). We investigate Holocene dust emission, transport and deposition explicitly as a function of Saharan land surface characteristics. To quantify changes in marine dust deposition, we perform equilibrium simulations of the mid-Holocene ($6k$) and pre-industrial ($0k$) dust cycle using the coupled climate-aerosol model ECHAM6-HAM2.1. The investigations are guided by the following questions: Can we support the interpretation of enhanced dust accumulation seen in the marine sediment cores as a consequence of changes in North African landscape? Or can already changes in climate alone explain these observations? Technically, we separate the importance of land surface and climate on dust emission and deposition following the factor separation method of Stein and Alpert (1993).

In Sect. 2, the model and the experimental setup is described. The model is evaluated by comparing present day global dust emission quantitatively and qualitatively with the AEROCOM Intercomparison study (Huneeus et al., 2011). Results are presented in Sect. 3. Simulated mid-Holocene and pre-industrial dust deposition rates are compared

CPD
11, 5269–5306, 2015

to those indicated from marine sediment records along the northwest African margin. A factor analysis is conducted to determine the influence and weighting of land surface conditions and orbital-forcing induced climate conditions, respectively. A discussion of the results, conclusions and suggestions for future studies follow in Sect. 4.

2 Experimental design

2.1 Model description

We employ the comprehensive climate-aerosol model ECHAM6-HAM2.1 (Stier et al., 2005) at a model resolution of T63L31 corresponding to a horizontal resolution of approximately $1.9^{\circ} \times 1.9^{\circ}$ and 31 vertical (hybrid)sigma-pressure levels in the atmosphere. Sea surface temperature (SST), sea ice cover (SIC), vegetation and lake cover are prescribed.

The aerosols included in the model are mineral dust, sulfate, black carbon, organic carbon and sea salt. Here we focus only on the mineral dust cycle. We use a model version equivalent to Stanelle et al. (2014) where the standard version is extended to determine potential dust source areas directly depending on land surface cover. Potential dust source areas are regions where dust can be emitted if certain criteria are fulfilled (e.g. the wind velocity has to exceed a threshold). Stanelle et al. (2014) define several rules to identify potential dust source areas, for example dust can not be emitted from areas covered with lakes and only from regions with sparse vegetation, as grasses and shrubs, or no vegetation. The amount of emitted aeolian dust from potential dust source areas is calculated following Tegen et al. (2002). After exceeding a threshold friction wind velocity, dust fluxes increase nonlinearly as a function of wind velocity. The critical threshold depends on particle size, soil moisture and texture (Marticorena and Bergametti, 1995). Additionally, the role of dry paleolakes as preferential sources of dust is accounted for in the model. Aerosol transport and interaction with

CPD
11, 5269–5306, 2015

the atmosphere is calculated according to Stier et al. (2005). Dust is removed from the atmosphere via dry deposition, wet deposition or sedimentation.

2.2 Model validation

Within the framework of the AEROCOM global dust model intercomparison project, the results of several global aerosols models are compared to observations to detect uncertainties and shortcomings in the simulation of the global dust cycle under present day climate (Huneeus et al., 2011). There still remain large uncertainties in modeling the global dust cycle. Among the models, simulated dust emission, deposition and the atmospheric burden vary by about an order of magnitude, for example emissions in North Africa range from 204 to 2888 $\mathrm{Tg\,a^{-1}}$. For comparison with the results from AEROCOM, we perform a simulation under present day conditions (averaged for the years 2000–2009; Table 1). Emission and deposition fluxes as well as the atmospheric burden are within the range of the AEROCOM results, but results of the ECHAM-HAM model are found to be lower than the AEROCOM median in general (Table 1). A detailed evaluation of the current model version is presented by Stanelle et al. (2014).

2.3 Experimental setup

We perform equilibrium simulations to study the mid-Holocene ($6k$) and pre-industrial ($0k$) global dust cycle. The main setup consists of four experiments (Table 2) to (1) compare with marine sediment records for both $6k$ and $0k$ (Sect. 3.1) and (2) identify the drivers of a change in dust flux between $6k$ and $0k$ (Sect. 3.2). Thereby, we separate two factors: (a) Saharan land surface conditions (vegetation cover and lake surface area) and (b) atmosphere–ocean conditions including orbital forcing, sea surface temperature and sea ice cover.

AO refers to atmosphere and ocean conditions. Orbital parameters are adapted to $0k$ and $6k$ respectively following Berger (1978) (Table 3). Prescribed sea surface temperature and sea ice cover for the pre-industrial era and the mid-Holocene respectively

CPD
11, 5269–5306, 2015

are taken from CMIP5 simulation runs with MPI-ESM (Giorgetta et al., 2013). The setup is defined following the CMIP5 protocol (Taylor et al., 2011). LV defines land surface conditions including lake and vegetation cover. Mid-Holocene vegetation cover reconstruction in North Africa (17° W–40° E; 10–30° N) is based on a vegetation map of Hoelzmann et al. (1998). In this approach, pollen data is linked to corresponding biomes (e.g. steppe and savanna). In the land surface component JSBACH of ECHAM, biomes are represented as a composition of plant functional types (PFT). Vegetation fraction and cover fractions of all eleven PFTs, surface albedo and water conductivity are set accordingly (Hagemann, 2002). Pre-industrial and reconstructed mid-Holocene vegetation fraction are plotted in Fig. 1. During the mid-Holocene the extent of lakes was much more pronounced than it is today (Hoelzmann et al., 1998; Gasse, 2000). Thus, the fractional lake mask in the model is adapted to a reconstruction of paleolakes from Tegen et al. (2002) (see Fig. 1 for $0k$ and $6k$ lake fraction).

In addition to the main simulations, we perform two simulations to separate the effect of altering vegetation and lake cover under mid-Holocene atmosphere–ocean conditions. In the fifth simulation, $AO_{6k}L_{0k}V_{6k}$, mid-Holocene vegetation is set and paleolakes are neglected. In the sixth simulation, $AO_{6k}L_{6k}V_{0k}$, only paleolakes are considered, whereas vegetation cover is set to the pre-industrial state (Table 2).

Each simulation is run for 31 years including one year of spin-up time. Thus, all results refer to an average of 30 years. The $6k$ setup, including orbital forcing parameters and greenhouse gases, is following the PMIP project standards (Harrison et al., 2001); Table 3. $0k$ and $6k$ greenhouse gas concentrations of CO_2, CH_4 and N_2O are set equally to $6k$ values of the PMIP protocol. The control run is denoted by $AO_{0k}LV_{0k}$.

3 Results

The Sahara is today one of the largest dust sources worldwide, which is recaptured by our simulations depicted in Fig. 2. In agreement with satellite data (Middleton and Goudie, 2001; Engelstaedter and Washington, 2007), we find especially the dry non-

CPD
11, 5269–5306, 2015

vegetated areas in Western Africa and the Bodélé Depression in the central Sahara to be highly productive dust sources. The patterns of deviations in dust emission between the 6k simulation and the pre-industrial control are clearly related to differences in lake fraction, which we show in Sect. 2 (Fig. 1, bottom). Obviously, during the mid-Holocene no dust could be emitted from areas covered with lakes, e.g. lake Mega-Chad covered the area where we find the Bodélé Depression today (Schuster et al., 2005). Also in West Africa smaller lakes and wetlands were widespread preventing dust emission. In contrast, areas with low stature vegetation allow for some dust emission.

While land surface conditions were modified solely in North Africa, we notice a small area with changing dust emission in the south of the Arabian peninsula and dust depositions expanding from the south of the Arabian peninsula to the Himalaya. Detailed investigations (not shown here) reveal that these anomalies only appear during boreal summer and we conclude that they are a consequence of a changed West African summer monsoon and corresponding wind patterns (Kutzbach and Otto-Bliesner, 1982; Weldeab et al., 2007).

Simulated deposition patterns in Fig. 2 reveal that Saharan dust is transported across the Atlantic to the Amazon basin for 0k. They are in agreement with patterns from other modeling studies for the pre-industrial era (Tegen et al., 2002; Mahowald et al., 1999).

3.1 Dust deposition rates in the North Atlantic: comparison with marine sediment records

We verify our simulation results by comparing with data from marine sediment cores for the pre-industrial control (experiment $AO_{0k}L_{0k}$; referred to as 0k) and for the mid-Holocene (experiment $AO_{6k}L_{6k}$; referred to as 6k). An evaluation for both time slices is important because we are interested in differences in dust flux between 0k and 6k.

Numerous studies of marine sediment records provide data of dust deposition rates in the North Atlantic Ocean which are comparable to our pre-industrial control simulation (see Table 4 and Fig. 3 for site locations). Only two studies present transient Holocene records of lithogenic dust fluxes in the Atlantic along the northwest African

CPD
11, 5269–5306, 2015

margin between 19 and 31° N (DeMenocal et al., 2000; McGee et al., 2013). They found large differences in dust accumulation between the mid-Holocene and the pre-industrial era.

We obtain simulated dust deposition rates in the grid cell whose midpoint is closest to the corresponding site location. The order of magnitude of the simulated fluxes is in agreement with data for both 0*k* and 6*k* (Fig. 4). For the mid-Holocene, slightly higher values are found in our simulations compared to marine sediment cores by McGee et al. (2013). The spatial log correlation coefficient of observed and modeled values at different sites (Fig. 3) is 0.8 for 0*k* and 0.64 for 6*k*. Exceptional high dust deposition rates were found both for 0*k* and for 6*k* at Site ODP 658 by Tiedemann et al. (1989) and DeMenocal et al. (2000). Compared to surrounding sites, about five to ten times more dust was deposited here due to enhanced supply of fluvial deposits additional to the high supply of eolian dust from the Sahara (Tiedemann et al., 1989). This local anomaly is not captured by the global model causing deviations between data and simulations results for site ODP 658. When neglecting this site, correlation coefficients increase to 0.88 and 0.96 respectively.

According to our 0*k* simulation, dust fluxes vary between 5.1 and 18.5 $g\,m^{-2}\,a^{-1}$ compared to an observed data range of 3.4 to 22 $g\,m^{-2}\,a^{-1}$. For 6*k*, they vary between 2.5 and 6 $g\,m^{-2}\,a^{-1}$ compared to 0.92 to 4.1 $g\,m^{-2}\,a^{-1}$ in the sediment cores (Table 5). In order to analyze changes in dust deposition between the mid-Holocene and pre-industrial era, we calculate the ratio between the 0*k* and 6*k* simulated dust deposition rates corresponding to the sediment cores of McGee et al. (2013) (Table 5). The incremental factor of dust deposition between 0*k* and 6*k* varies from 2.1 to 3.1 and increases monotonously from north to south. McGee et al. (2013) estimate a ratio of about 5 between 0*k* and 6*k*, whereas a ratio of < 2 was found in the study of DeMenocal et al. (2000).

An increase of dust fluxes from north to south was observed by McGee et al. (2013). This is also seen in our model results (Fig. 5). To determine the north-south gradient, simulated dust deposition rates in the three ocean grid cells that are closest to the

CPD
11, 5269–5306, 2015

northwest African margin between 19 and 27° N are considered (Fig. 5). We interpolate the simulated dust depositions as a function of latitude linearly applying the least square method (straight line in Fig. 5). For $0k$, simulated dust deposition rates increase thus by $1.76\,g\,m^{-2}\,a^{-1}$ per degree latitude; for $6k$, they increase by $0.67\,g\,m^{-2}\,a^{-1}$ per degree latitude. The north-south gradient obtained from marine sediment core data (Table 4) differs slightly from ours with dust accumulation increasing by $2.47\,g\,m^{-2}\,a^{-1}$ per degree latitude for $0k$ and $0.52\,g\,m^{-2}\,a^{-1}$ per degree latitude for $6k$. The increase in dust deposition with decreasing latitude can tentatively be attributed to the wind climatology. According to the NCEP reanalysis (Kalnay et al., 1996), present day surface winds are increasing from north to south along the West African margin and can thus transport higher amounts of dust to the ocean.

3.2 Influence of land surface conditions and atmosphere–ocean conditions on dust emission, transport and deposition

The simulated dust emission, atmospheric burden, total deposition and precipitation in North Africa and the global life time of dust in the atmosphere for the conducted experiments are summarized in Table 6. Additionally, percentages of wet deposition, dry deposition and sedimentation of the total deposition are presented. Standard deviations of the 30 year dust emission ensemble are given.

Pre-industrial land surface conditions result in much higher dust emission compared to mid-Holocene land surface conditions. This is valid independently of atmospheric and ocean boundary conditions. Emissions are 3.3 to 3.8 times higher for AO_xLV_{0k} compared to AO_xLV_{6k} with $x \in \{0k, 6k\}$. Rates of deposition and the dust burden in the atmosphere increase by factor 2.1 to 2.3 and 2.5 to 2.8, respectively. When atmosphere and ocean are adjusted to $6k$ and the land surface is fixed to pre-industrial ($AO_{6k}LV_{0k}$), the dust cycle is enhanced only slightly compared to the pre-industrial control ($AO_{0k}LV_{0k}$). On the other hand, for mid-Holocene land surface cover (LV_{6k}), mid-Holocene atmosphere–ocean conditions reduce emission and enhance deposition slightly (compare $AO_{0k}LV_{6k}$ and $AO_{6k}LV_{6k}$ in Table 6).

CPD
11, 5269–5306, 2015

Is the suppression of dust emission by land surface conditions due to increased lake surface area or rather linked to enhanced vegetation cover? In experiments $AO_{6k}L_{0k}V_{6k}$ and $AO_{6k}L_{6k}V_{0k}$, we change lake and vegetation cover separately, one is set to 6*k* conditions, while the other one remains in the pre-industrial state, respectively. In either experiment, dust emission is approximately halved and deposition reduces to about 70 % compared to the pre-industrial control (compare Table 6). Emission and deposition fluxes are still higher than fluxes obtained with fully mid-Holocene land surface cover. The burden is slightly higher for $AO_{6k}L_{6k}V_{0k}$ compared to $AO_{6k}L_{0k}V_{6k}$. In conclusion, paleolakes and mid-Holocene vegetation contributed both and nearly to the same extent to a reduced dust cycle during the mid-Holocene.

Emission, transport and deposition of dust are closely linked to each other. Land surface characteristics and surface winds determine primarily the emission of dust. Furthermore, climatic conditions have an impact on dust transport and deposition. Differences in the type of deposition point to meteorological conditions. A higher fraction of wet deposition compared to dry deposition and sedimentation indicates enhanced rainfall. About 20.6 % of the simulated total deposition is due to wet deposition for the pre-industrial control ($AO_{0k}LV_{0k}$) compared to about 51.1 % for mid-Holocene conditions ($AO_{6k}LV_{6k}$) corresponding to increased annual rainfall from 0.66 to 1.97 mm day^{-1}. Consequently, the global life time of dust in the atmosphere decreases (from 4.4 to 3.7 days) when mid-Holocene land surface is prescribed because particles are washed out more rapidly from the atmosphere. This result is almost unaffected by a change in orbit and ocean conditions. Only about 41 % of Saharan dust is deposited in the emission area for pre-industrial conditions. Hence, a large quantity of dust is transported beyond North Africa to the North Atlantic and even to the Amazon area as seen in Fig. 2. In contrast, the ratio of deposited vs. emitted dust in North Africa is about 75 % for mid-Holocene conditions, which is related to shorter life times, enhanced rainfall and a higher impact of wet deposition.

CPD
11, 5269–5306, 2015

3.3 Factor analysis of controls on dust emission and deposition

To isolate the impacts of (a) land surface conditions and (b) atmosphere–ocean conditions on dust emission in North Africa and deposition fluxes in the North Atlantic along the northwest African margin, we apply the factor separation method of Stein and Alpert (1993) to the four main simulations $AO_{0k}LV_{0k}$, $AO_{6k}LV_{0k}$, $AO_{0k}LV_{6k}$ and $AO_{6k}LV_{6k}$. We explain the methodology exemplified for dust emission. Dust emission in North Africa is defined as

$$f(s) = \int_{10^\circ\,\mathrm{N}}^{30^\circ\,\mathrm{N}} \int_{17^\circ\,\mathrm{W}}^{40^\circ\,\mathrm{E}} e_s(x,y)\mathrm{d}x\mathrm{d}y, \quad s \in \{AO_{0k}LV_{0k}, AO_{6k}LV_{0k}, AO_{0k}LV_{6k}, AO_{6k}LV_{6k}\}, \tag{1}$$

where $e_s(x,y)$ is the simulated dust emission at point (x,y) for simulation s.

The total difference in dust emission in North Africa between $6k$ and $0k$

$$\Delta_{6k-0k} = f(AO_{6k}LV_{6k}) - f(AO_{0k}LV_{0k}), \tag{2}$$

is divided into three components

$$\Delta_{6k-0k} = \Delta_{AO} + \Delta_{LV} + \Delta_{SYN}. \tag{3}$$

The contribution Δ_{AO} due to differences in orbital forcing, sea surface temperature and sea ice cover and the contribution Δ_{LV}, which captures the effects of changed land surface cover, are given by

$$\Delta_{AO} = f(AO_{6k}LV_{0k}) - f(AO_{0k}LV_{0k}), \tag{4}$$
$$\Delta_{LV} = f(AO_{0k}LV_{6k}) - f(AO_{0k}LV_{0k}). \tag{5}$$

The synergy between both factors reads

$$\Delta_{SYN} = f(AO_{6k}LV_{6k}) - f(AO_{0k}LV_{0k}) - (\Delta_{AO} + \Delta_{LV}) \tag{6}$$

CPD
11, 5269–5306, 2015

$$= f(AO_{6k}LV_{6k}) - f(AO_{6k}LV_{0k}) - f(AO_{0k}LV_{6k}) + f(AO_{0k}LV_{0k}). \quad (7)$$

In Table 7 the total difference Δ_{6k-0k} and the percentages of Δ_{AO}, Δ_{LV} and Δ_{SYN} are presented for dust emission in North Africa and deposition along the northwest African margin. Differences due to changes in land surface conditions Δ_{LV} differ not more than 5 % from the total differences Δ_{6k-0k}. We conclude that land surface cover was the main control on dust emission in North Africa and associated deposition along the northwest African margin during the mid-Holocene. The impact of atmosphere–ocean conditions Δ_{AO} is even slightly negative for dust emission and has a negative effect of 16.5 % of the total differences for dust deposition in the North Atlantic. The synergy effect is 7.6 % for dust emission and 20.4 % for dust deposition.

Comparing patterns of dust emission in North Africa (Fig. 6) and dust deposition in the North Atlantic (Fig. 7) visually, emphasizes the high impact of land surface conditions. The patterns of the contribution Δ_{LV} and the total difference Δ_{6k-0k} are almost identical. Mid-Holocene atmosphere–ocean conditions with fixed pre-industrial land surface ($AO_{6k}L_{0k}$) lead to a change in dust emission only locally. Interestingly, there is an increase in dust emission from the Western Sahara, whereas less dust is emitted from the Bodélé Depression. Dust deposition in the North Atlantic does not differ much from the control and is even slightly enhanced between 10 and 15° N. The change in dust sources and deposition patterns is linked to a changed seasonal cycle (see Appendix).

Relating Fig. 6 to Fig. 7, this analysis demonstrates that emission in North Africa is directly linked to deposition in the North Atlantic along the northwest African margin. We find land surface conditions to be the main control on dust emission and deposition with a contribution of more than 95 %. Distraction of dust transport due to changes in atmospheric processes play a minor role.

CPD
11, 5269–5306, 2015

4 Discussion and conclusion

We have explored the question whether variations in North African land surface cover resulted in a significant difference in dust deposition fluxes in the North Atlantic Ocean between the pre-industrial (1850 AD) and mid-Holocene (6 ka BP) as indicated by marine sediments (McGee et al., 2013; DeMenocal et al., 2000). Therefore, we have simulated the dust cycle for both eras. We have analyzed the contribution of a change in land surface conditions, including vegetation cover and lake surface area, and the contribution of differing atmosphere–ocean conditions to a difference in dust emission and deposition between the mid-Holocene and the pre-industrial control. In our simulations, orbital forcing parameters and ocean conditions are adjusted respectively and mid-Holocene land surface conditions are fixed according to vegetation reconstructions of Hoelzmann et al. (1998) and simulations of lake surface area (Tegen et al., 2002).

Our simulation results support the hypothesis of decreased dust activity in North Africa during the African Humid Period (AHP) at 6 ka BP compared to pre-industrial times with reduced dust emission fluxes from the Saharan desert and an associated decrease of dust accumulation in the North Atlantic. Simulated dust emission fluxes are reduced to about 27 % of pre-industrial fluxes and simulated deposition fluxes are lower by a factor between 2.1 and 3.1 for specific site locations. Marine sediment records indicate lower deposition fluxes for the mid-Holocene compared to pre-industrial by factors between about two (DeMenocal et al., 2000) and five (McGee et al., 2013). For the mid-Holocene, we find deposition rates in the North Atlantic slightly higher than indicated by McGee et al. (2013), resulting in a somewhat lower contrast when compared with pre-industrial fluxes. However, within a range of uncertainty and with respect to magnitude and sign, our simulation results are in agreement with data from marine cores for pre-industrial and mid-Holocene times. Ratmeyer et al. (1999) argued that in the area of the chosen cores, there is a fast and mostly undisturbed downward transport of lithogenic material in the water column. Thus, sedimentation fluxes mostly correlate well between upper and lower ocean depths and the surface. A particular

CPD
11, 5269–5306, 2015

exception are fluxes at site ODP 658: they are found to be five to ten times larger than those from surrounding sites. Tiedemann et al. (1989) suggest additional fluvial inputs are responsible for the deviation. Further, we find a north-south increase of dust deposition rates along the northwest African margin during the mid-Holocene and pre-industrial era, which is consistent with observations of McGee et al. (2013).

We identify land surface cover to be the main control on dust emission in North Africa and associated dust deposition in the North Atlantic. Differences in lake surface area and vegetation cover respectively appear to contribute by about the same amount to the reduced dust cycle of the mid-Holocene. Atmosphere–ocean conditions only affect the total amount of emitted and deposited dust only marginally. They have, however, an impact on the seasonal dust cycle and dust source regions.

By explicitly modeling global dust emission, transport and deposition, our results add additional confidence to the hypothesis that higher sedimentation rates during the early to mid-Holocene in marine sediment cores close to the northwest African margin must be interpreted as a result of either more extensive vegetation ("green Sahara"), a result of extended paleolakes or a combination of both.

The issue of the abruptness of increased dust accumulation in the marine cores during the Holocene remains to be solved. Do land surface–climate feedbacks generate a sudden reduction of vegetation cover or lake surface area, resulting in an abrupt exposure of dust source areas? Or can the abrupt change in dust deposition in the North Atlantic be interpreted as a nonlinear response of Saharan dust emission to a steadily changing surface? Do multiple equilibria or bifurcations exist in the dynamic interaction of dust, vegetation and climate? These questions will have to be addressed by transient climate simulations including interactive vegetation and a scheme that dynamically simulates the extent of surface water areas following Stacke and Hagemann (2012) into the climate-aerosol model.

CPD
11, 5269–5306, 2015

Appendix: Wind patterns and annual cycle

An analysis of the seasonal cycle of dust emission in relation to meteorological conditions is provided to get a deeper understanding of our simulation results. We present the seasonal cycle of dust emission for all experiments and relate them to seasonal wind patterns.

North African dust emission is linked to a distinct seasonal cycle (Engelstaedter and Washington, 2007). Northeasterly near surface trade winds below 1000 m height are responsible for the majority of dust transport from the Saharan desert toward the North Atlantic during the winter months (Ratmeyer et al., 1999; Engelstaedter and Washington, 2007). In our simulations, northeasterly winds are strongest along the coast during winter (Fig. 8). Accordingly, maximum dust emission rates occur from January till April (Fig. 9). Dust production in the Western Sahara becomes active towards summer. Dust is then lifted up and transported by the Harmattan or Saharan Air Layer (SAL) (Carlson and Prospero, 1972), that is coupled to the African Easterly Jet at 1000 to 5000 m height (Tiedemann et al., 1989). Accordingly, the convergence belt is shifted northwards during boreal summer. We notice a second smaller peak of dust emission around June in the control run. Dust activity is decreasing at the end of the year in all regions (Fig. 9). The Bodélé Depression in central Chad is active throughout most of the year. In this region, dust is emitted and lifted up by Harmattan winds.

Mid-Holocene wind patterns hardly change during winter compared to the pre-industrial control, whereas during the summer months the ITCZ propagates further north (Fig. 8). Wind fields from the Eastern Atlantic ocean to the Sahel area in the southwest induced by the West African monsoon extent further north. Consequently, the transport of dust from North Africa to the North Atlantic is reduced.

If orbital forcing is adjusted to mid-Holocene conditions and pre-industrial land surface is kept ($AO_{6k}LV_{0k}$), we obtain only a slight increase in annual dust emission (Sect. 3.2) in our simulations, but the seasonal cycle changes significantly (Fig. 9, bottom left). The corresponding patterns of simulated dust emission show an enhanced

CPD
11, 5269–5306, 2015

dust productivity in the Western Sahara compared to the control run (Sect. 3.3), where dust productivity increases toward the summer (Engelstaedter and Washington, 2007). Accordingly, dust emission is highest during summer in our simulation (June to August). Though the total amount of annual dust emission hardly changes, there is a clear shift in source regions and the seasonal cycle, when only mid-Holocene atmosphere–ocean conditions are set. Dust emission is strongly prevented throughout the year, when mid-Holocene vegetation and lakes are prescribed (LV_{6k}). Hereby, the seasonal cycle of dust emission is closely linked to the seasonal plant growth. The leaf area index and the soil moisture increase during the summer months, when the West African monsoon becomes active. Though, the change of atmosphere–ocean conditions from $0k$ to $6k$ tends to shift the time of maximal dust productivity from March–May to May–July (compare $AO_{0k}LV_{6k}$ and $AO_{6k}LV_{6k}$).

The analysis of the seasonal cycle of dust emission shows that mid-Holocene land surface cover suppresses dust emission throughout the year, what results in reduced annual dust emission. Although mid-Holocene atmosphere–ocean conditions do not provoke a significant change of the total annual amount of emitted dust in North Africa, they affect the atmospheric circulation, what is reflected in a changed seasonal cycle and a shift of dust source regions.

Acknowledgements. We thank Stefan Hagemann for review and Andrea Kay for spelling correction.

The article processing charges for this open-access publication
were covered by the Max Planck Society.

References

Adkins, J., DeMenocal, P., and Eshel, G.: The "African Humid Period" and the record of marine upwelling from excess 230Th in ODP hole 658C, Paleoceanography, 21, PA4203, doi:10.1029/2005PA001200, 2006. 5271

CPD
11, 5269–5306, 2015

Albani, S., Mahowald, N. M., Winckler, G., Anderson, R. F., Bradtmiller, L. I., Delmonte, B., François, R., Goman, M., Heavens, N. G., Hesse, P. P., Hovan, S. A., Kohfeld, K. E., Lu, H., Maggi, V., Mason, J. A., Mayewski, P. A., McGee, D., Miao, X., Otto-Bliesner, B. L., Perry, A. T., Pourmand, A., Roberts, H. M., Rosenbloom, N., Stevens, T., and Sun, J.: Twelve thousand years of dust: the Holocene global dust cycle constrained by natural archives, Clim. Past Discuss., 10, 4277–4363, doi:10.5194/cpd-10-4277-2014, 2014. 5271

Armitage, S. J., Bristow, C. S., and Drake, N. A.: West African monsoon dynamics inferred from abrupt fluctuations of Lake Mega-Chad, P. Natl. Acad. Sci. USA, 112, 8543–8548, doi:10.1073/pnas.1417655112, 2015. 5271

Berger, A.: Long-term variations of daily insolation and quaternary climatic changes, J. Atmos. Sci., 35, 2362–2367, 1978. 5270, 5274, 5293

Bory, A. J.-M., and Newton, P. P.: Transport of airborne lithogenic material down through the water column in two contrasting regions of the eastern subtropical North Atlantic Ocean, Global Biogeochem. Cy., 14, 297–315, doi:10.1029/1999GB900098, 2000. 5294

Brovkin, V., Claussen, M., Petoukhov, V., and Ganopolski, A.: On the stability of the atmosphere-vegetation system in the Sahara/Sahel region, J. Geophys. Res.-Atmos., 103, 31613–31624, doi:10.1029/1998JD200006, 1998. 5271

Carlson, T. and Prospero, J.: The large-scale movement of Saharan Air outbreaks over the Northern Equatorial Atlantic, J. Appl. Meteorol., 11, 283–297, 1972. 5284

Claussen, M., Kubatzki, C., Brovkin, V., Ganopolski, A., Hoelzmann, P., and Pachur, H.-J.: Simulation of an abrupt change in Saharan vegetation in the Mid-Holocene, Geophys. Res. Lett., 26, 2037–2040, doi:10.1029/1999GL900494, 1999. 5271

Cockerton, H. E., Holmes, J. A., Street-Perrott, F. A., and Ficken, K. J.: Holocene dust records from the West African Sahel and their implications for changes in climate and land surface conditions, J. Geophys. Res.-Atmos., 119, 8684–8694, doi:10.1002/2013JD021283, 2014. 5271

DeMenocal, P., Ortiz, J., Guilderson, T., Adkins, J., Sarnthein, M., Baker, L., and Yarusinsky, M.: Abrupt onset and termination of the African Humid Period: rapid climate responses to gradual insolation forcing, Quaternary Sci. Rev., 19, 347–361, 2000. 5271, 5272, 5277, 5282, 5294

Engelstaedter, S. and Washington, R.: Atmospheric controls on the annual cycle of North African dust, J. Geophys. Res.-Atmos., 112, D03103, doi:10.1029/2006JD007195, 2007. 5275, 5284, 5285

CPD
11, 5269–5306, 2015

Fischer, G., Donner, B., Ratmeyer, V., Davenport, R., and Wefer, G.: Distinct year-to-year flux variations off Cape Blanc during 1988–1991: relation to 18O-deduced sea-surface temperatures and trade winds, J. Mar. Res., 54, 73–98, 1996. 5294

Gasse, F.: Hydrological changes in the African tropics since the last glacial maximum, Quaternary Sci. Rev., 19, 189–211, doi:10.1016/S0277-3791(99)00061-X, 2000. 5275

Giorgetta, M. A., Jungclaus, J., Reick, C. H., Legutke, S., Bader, J., Böttinger, M., Brovkin, V., Crueger, T., Esch, M., Fieg, K., Glushak, K., Gayler, V., Haak, H., Hollweg, H.-D., Ilyina, T., Kinne, S., Kornblueh, L., Matei, D., Mauritsen, T., Mikolajewicz, U., Mueller, W., Notz, D., Pithan, F., Raddatz, T., Rast, S., Redler, R., Roeckner, E., Schmidt, H., Schnur, R., Segschneider, J., Six, K. D., Stockhause, M., Timmreck, C., Wegner, J., Widmann, H., Wieners, K.-H., Claussen, M., Marotzke, J., and Stevens, B.: Climate and carbon cycle changes from 1850 to 2100 in MPI-ESM simulations for the Coupled Model Intercomparison Project phase 5, J. Adv. Model. Earth Sys., 5, 572–597, doi:10.1002/jame.20038, 2013. 5275

Hagemann, S.: An improved land surface parameter dataset for global and regional climate models, MPI Report No. 289, Max Planck Institute for Meteorology, Hamburg, 2002. 5275

Harrison, S. P., Kohfeld, K. E., Roelandt, C., and Claquin, T.: The role of dust in climate changes today, at the last glacial maximum and in the future, Earth-Sci. Rev., 54, 43–80, doi:10.1016/S0012-8252(01)00041-1, 2001. 5275, 5293

Hoelzmann, P., Jolly, D., Harrison, S. P., Laarif, F., Bonnefille, R., and Pachur, H.-J.: Mid-Holocene land-surface conditions in northern Africa and the Arabian Peninsula: a data set for the analysis of biogeophysical feedbacks in the climate system, Global Biogeochem. Cy., 12, 35–51, doi:10.1029/97GB02733, 1998. 5271, 5272, 5275, 5282, 5298

Huneeus, N., Schulz, M., Balkanski, Y., Griesfeller, J., Prospero, J., Kinne, S., Bauer, S., Boucher, O., Chin, M., Dentener, F., Diehl, T., Easter, R., Fillmore, D., Ghan, S., Ginoux, P., Grini, A., Horowitz, L., Koch, D., Krol, M. C., Landing, W., Liu, X., Mahowald, N., Miller, R., Morcrette, J.-J., Myhre, G., Penner, J., Perlwitz, J., Stier, P., Takemura, T., and Zender, C. S.: Global dust model intercomparison in AeroCom phase I, Atmos. Chem. Phys., 11, 7781–7816, doi:10.5194/acp-11-7781-2011, 2011. 5272, 5274, 5291

Jickells, T., Newton, P., King, P., Lampitt, R., and Boutle, C.: A comparison of sediment trap records of particle fluxes from 19 to 48° N in the northeast Atlantic and their relation to surface water productivity, Deep-Sea Res. Pt. I, 43, 971–986, doi:10.1016/0967-0637(96)00063-5, 1996. 5294

CPD
11, 5269–5306, 2015

Jolly, D., Prentice, I. C., Bonnefille, R., Ballouche, A., Bengo, M., Brenac, P., Buchet, G., Burney, D., Cazet, J.-P., Cheddadi, R., Edorh, T., Elenga, H., Elmoutaki, S., Guiot, J., Laarif, F., Lamb, H., Lezine, A.-M., Maley, J., Mbenza, M., Peyron, O., Reille, M., Reynaud-Farrera, I., Riollet, G., Ritchie, J. C., Roche, E., Scott, L., Ssemmanda, I., Straka, H., Umer, M., Van Campo, E., Vilimumbalo, S., Vincens, A., and Waller, M.: Biome reconstruction from pollen and plant macrofossil data for Africa and the Arabian peninsula at 0 and 6000 years, J. Biogeogr., 25, 1007–1027, doi:10.1046/j.1365-2699.1998.00238.x, 1998. 5271, 5272

Kalnay, E., Kanamitsu, M., Kistler, R., Collins, W., Deaven, D., Gandin, L., Iredell, M., Saha, S., White, G., Woollen, J., Zhu, Y., Leetmaa, A., Reynolds, R., Chelliah, M., Ebisuzaki, W., Higgins, W., Janowiak, J., Mo, K. C., Ropelewski, C., Wang, J., Jenne, R., and Joseph, D.: The NCEP/NCAR 40-year reanalysis project, B. Am. Meteorol. Soc., 77, 437–471, 1996. 5278

Kohfeld, K. and Harrison, S.: How well can we simulate past climates? Evaluating the models using global palaeoenvironmental datasets, Quaternary Sci. Rev., 19, 321–346, doi:10.1016/S0277-3791(99)00068-2, 2000. 5271

Kremling, K. and Streu, P.: Saharan dust influenced trace element fluxes in deep North Atlantic subtropical waters, Deep-Sea Res. Pt. I, 40, 1155–1168, doi:10.1016/0967-0637(93)90131-L, 1993. 5294

Kröpelin, S., Verschuren, D., Lézine, A.-M., Eggermont, H., Cocquyt, C., Francus, P., Cazet, J.-P., Fagot, M., Rumes, B., Russell, J. M., Darius, F., Conley, D. J., Schuster, M., von Suchodoletz, H., and Engstrom, D. R.: Climate-driven ecosystem succession in the Sahara: the past 6000 years, Science, 320, 765–768, doi:10.1126/science.1154913, 2008. 5271

Kutzbach, J. E.: Monsoon climate of the early Holocene: climate experiment with the Earth's orbital parameters for 9000 years ago, Science, 214, 59–61, doi:10.1126/science.214.4516.59, 1981. 5270

Kutzbach, J. E. and Otto-Bliesner, B. L.: The sensitivity of the african-asian monsoonal climate to orbital parameter changes for 9000 years b.p. in a low-resolution general circulation model, J. Atmos. Sci., 39, 1177–1188, 1982. 5276

Kutzbach, J. E. and Street-Perrott, F. A.: Milankovitch forcing of fluctuations in the level of tropical lakes from 18 to 0 kyr BP, Nature, 317, 130–134, 1985. 5271

Mahowald, N., Kohfeld, K., Hansson, M., Balkanski, Y., Harrison, S. P., Prentice, I. C., Schulz, M., and Rodhe, H.: Dust sources and deposition during the last glacial maximum and current climate: a comparison of model results with paleodata from ice cores and ma-

CPD
11, 5269–5306, 2015

rine sediments, J. Geophys. Res.-Atmos., 104, 15895–15916, doi:10.1029/1999JD900084, 1999. 5276
Marticorena, B. and Bergametti, G.: Modeling the atmospheric dust cycle: 1. Design of a soil-derived dust emission scheme, J. Geophys. Res.-Atmos., 100, 16415–16430, doi:10.1029/95JD00690, 1995. 5273
McGee, D., deMenocal, P., Winckler, G., Stuut, J., and Bradtmiller, L.: The magnitude, timing and abruptness of changes in North African dust deposition over the last 20,000 yr, Earth Planet. Sc. Lett., 371–372, 163–176, doi:10.1016/j.epsl.2013.03.054, 2013. 5271, 5272, 5277, 5282, 5283, 5294
Middleton, N. J. and Goudie, A. S.: Saharan dust: sources and trajectories, T. I. Brit. Geogr., 26, 165–181, doi:10.1111/1475-5661.00013, 2001. 5275
Prentice, I. C., Jolly, D., and 6000 Participants, B.: Mid-Holocene and glacial-maximum vegetation geography of the northern continents and Africa, J. Biogeogr., 27, 507–519, 2000. 5271
Ratmeyer, V., Fischer, G., and Wefer, G.: Lithogenic particle fluxes and grain size distributions in the deep ocean off northwest Africa: implications for seasonal changes of aeolian dust input and downward transport, Deep-Sea Res. Pt. I, 46, 1289–1337, doi:10.1016/S0967-0637(99)00008-4, 1999. 5282, 5284, 5294
Schuster, M., Roquin, C., Duringer, P., Brunet, M., Caugy, M., Fontugne, M., Mackaye, H. T., Vignaud, P., and Ghienne, J.-F.: Holocene Lake Mega-Chad palaeoshorelines from space, Quaternary Sci. Rev., 24, 1821–1827, doi:10.1016/j.quascirev.2005.02.001, 2005. 5271, 5276
Stacke, T. and Hagemann, S.: Development and evaluation of a global dynamical wetlands extent scheme, Hydrol. Earth Syst. Sci., 16, 2915–2933, doi:10.5194/hess-16-2915-2012, 2012. 5283
Stanelle, T., Bey, I., Raddatz, T., Reick, C., and Tegen, I.: Anthropogenically induced changes in twentieth century mineral dust burden and the associated impact on radiative forcing, J. Geophys. Res.-Atmos., 119, 13526–13546, doi:10.1002/2014JD022062, 2014. 5273, 5274
Stein, U. and Alpert, P.: Factor separation in numerical simulations, J. Atmos. Sci., 50, 2107–2115, 1993. 5272, 5280
Stier, P., Feichter, J., Kinne, S., Kloster, S., Vignati, E., Wilson, J., Ganzeveld, L., Tegen, I., Werner, M., Balkanski, Y., Schulz, M., Boucher, O., Minikin, A., and Petzold, A.: The aerosol-

CPD
11, 5269–5306, 2015

climate model ECHAM5-HAM, Atmos. Chem. Phys., 5, 1125–1156, doi:10.5194/acp-5-1125-2005, 2005. 5273, 5274
Street-Perrott, F., Marchand, D., Roberts, N., and Harrison, S. O. U. U. G. S.: Global lake-level variations from 18,000 to 0 years ago: a palaeoclimate analysis, Oxford University Press, New York, 1989. 5271
Sudarchikova, N., Mikolajewicz, U., Timmreck, C., O'Donnell, D., Schurgers, G., Sein, D., and Zhang, K.: Modelling of mineral dust for interglacial and glacial climate conditions with a focus on Antarctica, Clim. Past, 11, 765–779, doi:10.5194/cp-11-765-2015, 2015. 5271
Taylor, K. E., Stouffer, R., and Meehl, G.: An overview of CMIP5 and the experiment design, B. Am. Meteorol. Soc., 93, 485–498, 2011. 5275
Tegen, I., Harrison, S. P., Kohfeld, K., Prentice, I. C., Coe, M., and Heimann, M.: Impact of vegetation and preferential source areas on global dust aerosol: results from a model study, J. Geophys. Res.-Atmos., 107, AAC 14–1–AAC 14–27, doi:10.1029/2001JD000963, 2002. 5272, 5273, 5275, 5276, 5282, 5298
Tiedemann, R., Sarnthein, M., and Stein, R.: Climatic changes in the western Sahara: aeolo-marine sediment record of the last 8 million years (Sites 657–661), Proceedings ODP, Scientific Results, 108, 241–278, 1989. 5277, 5283, 5284, 5294
Weldeab, S., Lea, D. W., Schneider, R. R., and Andersen, N.: 155,000 years of West African monsoon and ocean thermal evolution, Science, 316, 1303–1307, doi:10.1126/science.1140461, 2007. 5276

CPD
11, 5269–5306, 2015

Table 1. Global dust emission, burden and deposition, and emission in North Africa (NA) from the AEROCOM models (Huneeus et al., 2011) including ECHAM5-HAM for the year 2000 and from ECHAM6-HAM2.1 averaged for 2000–2009. Uncertainties in the last two rows are standard deviations of the 10 year ensemble.

Model	Emission [Tga^{-1}]	Emission NA [Tga^{-1}]	Burden [Tg]	Wet Dep. [Tga^{-1}]	Dry Dep. [Tga^{-1}]	Sedi. [Tga^{-1}]
AEROCOM median	1123	792	15.8	357	396	314
(range)	(514–4313)	(204–2888)	(6.8–29.5)	(295–1382)	(37–2791)	(22–2475)
ECHAM5-HAM	664	401	8.28	374	37	265
(Stier et al., 2005)						
ECHAM6-HAM2.1	912	491	10.9	473	83	358
(Stanelle et al., 2014)	±77	±66				
this study,	797.5	420.2	9.9	419.6	74.8	306.1
ECHAM6-HAM2.1	±94.8	±75.6	±1.1	±47.4	±11.3	±39.9

CPD
11, 5269–5306, 2015

Table 2. Experimental setup including orbital parameters, sea surface temperature (SST) and sea ice cover (SIC), lake and vegetation cover; $0k$ refers to pre-industrial and $6k$ to mid-Holocene conditions. While differences in AO conditions apply globally, differences in L and V conditions apply only to the Saharan box (17° W–40° E; 10–30° N).

	Orbit	SST, SIC	Lakes	Vegetation
$AO_{0k}LV_{0k}$	$0k$	$0k$	$0k$	$0k$
$AO_{0k}LV_{6k}$	$0k$	$0k$	$6k$	$6k$
$AO_{6k}LV_{0k}$	$6k$	$6k$	$0k$	$0k$
$AO_{6k}LV_{6k}$	$6k$	$6k$	$6k$	$6k$
$AO_{6k}L_{0k}V_{6k}$	$6k$	$6k$	$0k$	$6k$
$AO_{6k}L_{6k}L_{0k}$	$6k$	$6k$	$6k$	$0k$

CPD
11, 5269–5306, 2015

Table 3. Orbital parameters derived from Berger (1978) and greenhouse gas concentrations following the PMIP protocol for 6*k* (Harrison et al., 2001).

	0*k* (pre-industrial)	6*k* (mid-Holocene)
Orbital parameters:		
Eccentricity	0.016715	0.018682
Obliquity (°)	23.441	24.105
Precession (°)	102.7	0.87
Greenhouse gases:		
CO_2 (ppm)	280	280
CH_4 (ppb)	650	650
N_2O (ppb)	270	270

CPD
11, 5269–5306, 2015

Table 4. Dust accumulation fluxes obtained from marine sediment cores close to the northwest African margin for 0k and 6k.

Marine sediment records						
No	Site	lat [° N]	lon [° E]	Acc. flux [$gm^{-2}\,a^{-1}$] 0k	6k	Reference
1	ODP 659	18.1	−21.0	14.7		Tiedemann et al. (1989)
2	BOFS-1	19.0	−20.17	21.55		Bory and Newton (2000)
3	CB2-1	21.15	−20.68	19.7		Fischer et al. (1996)
4	CB2-2	21.15	−20.69	20.48		Ratmeyer et al. (1999)
5	CI 1 upper	29.11	−15.45	4.15		Ratmeyer et al. (1999)
6	22N25W	21.93	−25.23	6.7		Kremling and Streu (1993); Jickells et al. (1996)
7	25N23W	24.55	−22.83	5.21		Jickells et al. (1996)
8	28N22W	28.00	−21.98	2.4		Jickells et al. (1996)
9	GC 68	19.36	−17.28	22.0	4.1	McGee et al. (2013)
10	ODP 658	20.75	−18.58	104.9	70	Tiedemann et al. (1989); DeMenocal et al. (2000)
11	GC 49	23.21	−17.85	5.5	1.2	McGee et al. (2013)
12	GC 37	26.82	−15.12	3.4	0.92	McGee et al. (2013)

CPD
11, 5269–5306, 2015

Table 5. Simulated dust deposition flux close to site *GC*37, *GC*49 and *GC*68 (Table 4) for 0*k* and 6*k* and the corresponding flux ratios between 0*k* and 6*k*.

	Simulated dust deposition flux close to site		
	*GC*37 [$g m^{-2} a^{-1}$]	*GC*49 [$g m^{-2} a^{-1}$]	*GC*68 [$g m^{-2} a^{-1}$]
0*k*	5.1	8.3	18.5
6*k*	2.5	3.7	6.0
ratio 0*k* : 6*k*	2.1	2.3	3.1

CPD
11, 5269–5306, 2015

Table 6. Dust emission, burden, deposition and precipitation in North Africa (17° W–40° E; 10–30° N) and global life time of dust for altering atmospheric and ocean (AO) and land surface conditions (LV).

Experiment	Emission [Tga^{-1}]	Burden [Tg]	Wet Dep. [%]	Dry Dep. [%]	Sedi. [%]	Total Dep. [Tga^{-1}]	Global life time [day]	Precip. [mm day^{-1}]
$AO_{0k}LV_{0k}$	352.6 ±44.3	2.62	20.6	9.6	69.8	144.9	4.4	0.66
$AO_{6k}LV_{0k}$	360.5 ±29.4	2.73	34.4	6.6	59.0	165.3	4.3	0.93
$AO_{0k}LV_{6k}$	107.8 ±12.3	1.04	43.4	4.7	51.9	70.2	3.7	1.79
$AO_{6k}LV_{6k}$	96.1 ±15.4	0.99	51.1	3.9	45.0	72.0	3.7	1.97
$AO_{6k}L_{0k}V_{6k}$	174.2 ±28.8	1.69	47.2	3.2	49.6	100.9	4.1	1.72
$AO_{6k}L_{6k}V_{0k}$	177.7 ±18.7	1.38	41.0	6.4	52.6	101.6	3.6	1.24

CPD
11, 5269–5306, 2015

Table 7. Total difference in dust emission in North Africa (17° W–40° E; 10–30° N) and dust deposition along the northwest African margin (30–17° W; 5–35° N) between 6*k* and 0*k* and percentages of land surface conditions, atmosphere–ocean conditions and synergy effects to the total difference.

	Δ_{6k-0k} [Tga^{-1}]	$\Delta_{AO}/\Delta_{6k-0k}$	$\Delta_{LV}/\Delta_{6k-0k}$	$\Delta_{SYN}/\Delta_{6k-0k}$
Emission	−256.5	−3.1 %	95.4 %	7.6 %
Deposition	−26.6	−16.5 %	96.1 %	20.4 %

CPD
11, 5269–5306, 2015

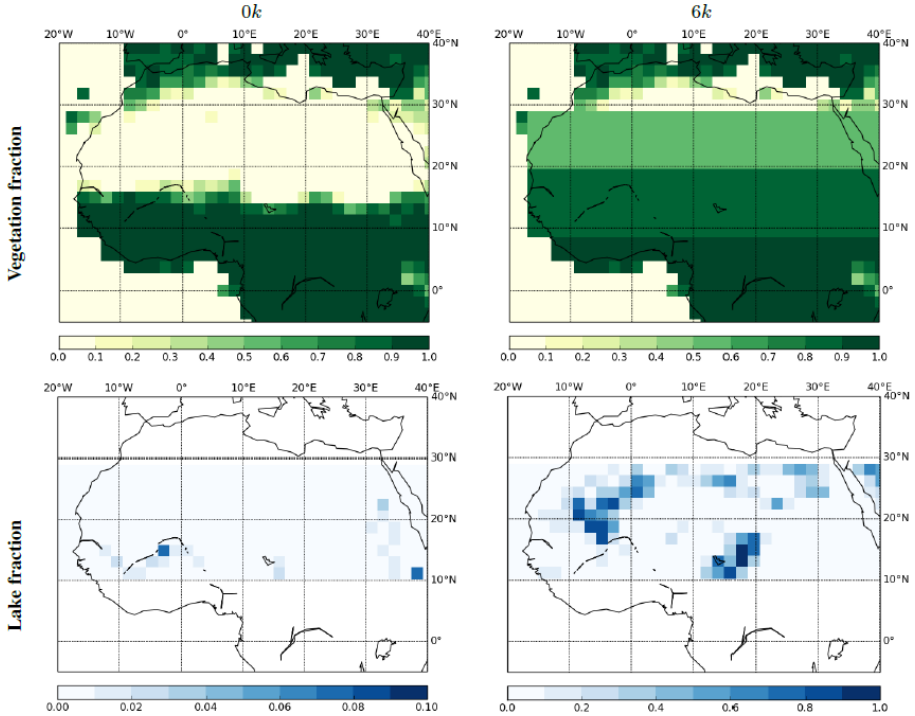

Figure 1. Vegetation and lake fraction for 0*k* and 6*k*. 6*k* lake fraction is obtained from Tegen et al. (2002) and 6*k* vegetation fraction is reconstructed following Hoelzmann et al. (1998). Note that lake fraction is scaled differently for 0*k* and 6*k*.

CPD
11, 5269–5306, 2015

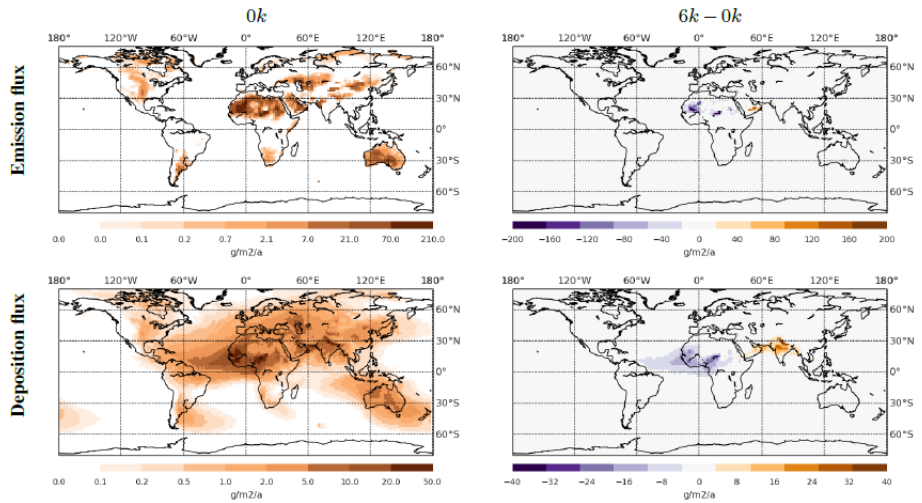

Figure 2. Simulated global annual mean dust emission flux (top) and dust deposition flux (bottom) for 0*k* (left) and for the difference 6*k* – 0*k* (right).

CPD
11, 5269–5306, 2015

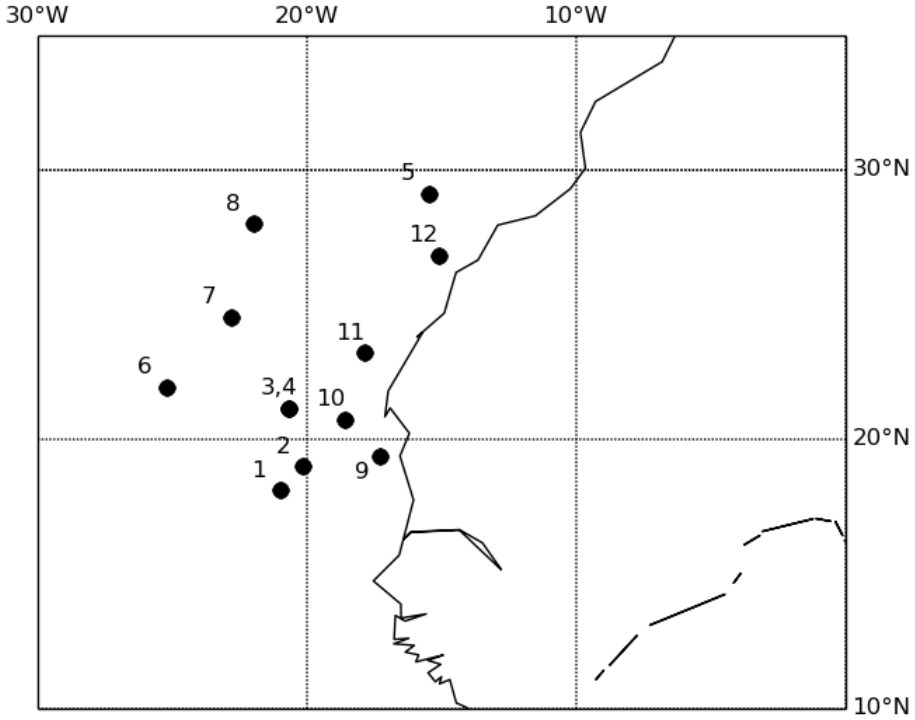

Figure 3. Site locations of marine sediment cores along the northwest African margin corresponding to Table 4.

CPD
11, 5269–5306, 2015

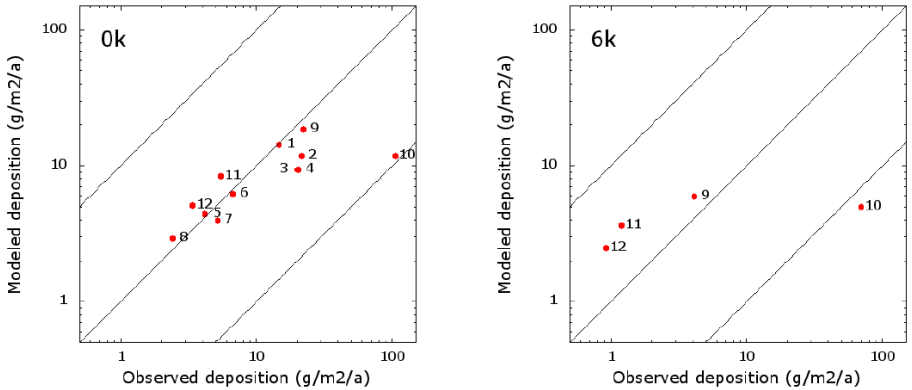

Figure 4. Simulated dust deposition flux for 0k (left, $AO_{0k}L_{0k}$) and 6k (right, $AO_{6k}L_{6k}$) compared with data from marine sediment cores (Table 4). Log correlation coefficients are: 0.8 (0k) and 0.64 (6k) (without ODP 658: 0.88 and 0.96).

CPD
11, 5269–5306, 2015

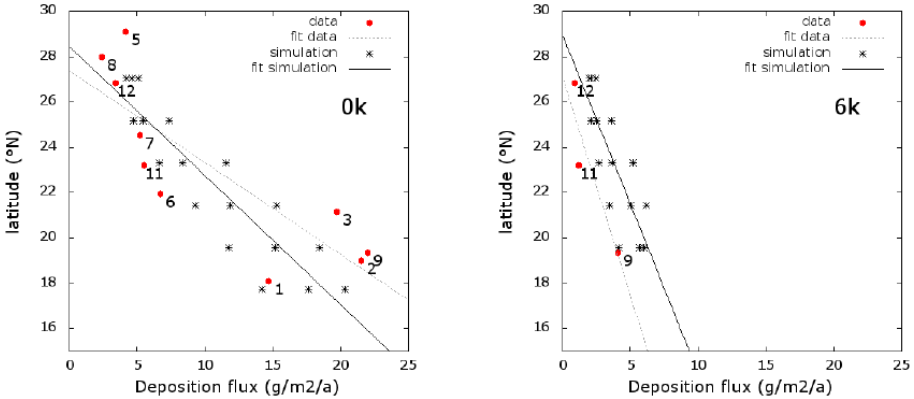

Figure 5. Simulated dust deposition flux for the three ocean grid cells that are closest to the northwest African margin for 0*k* (left) and 6*k* (right) at different latitudes compared with data from marine sediment cores (Table 4). The straight lines are linear interpolations obtained with the least square method.

CPD
11, 5269–5306, 2015

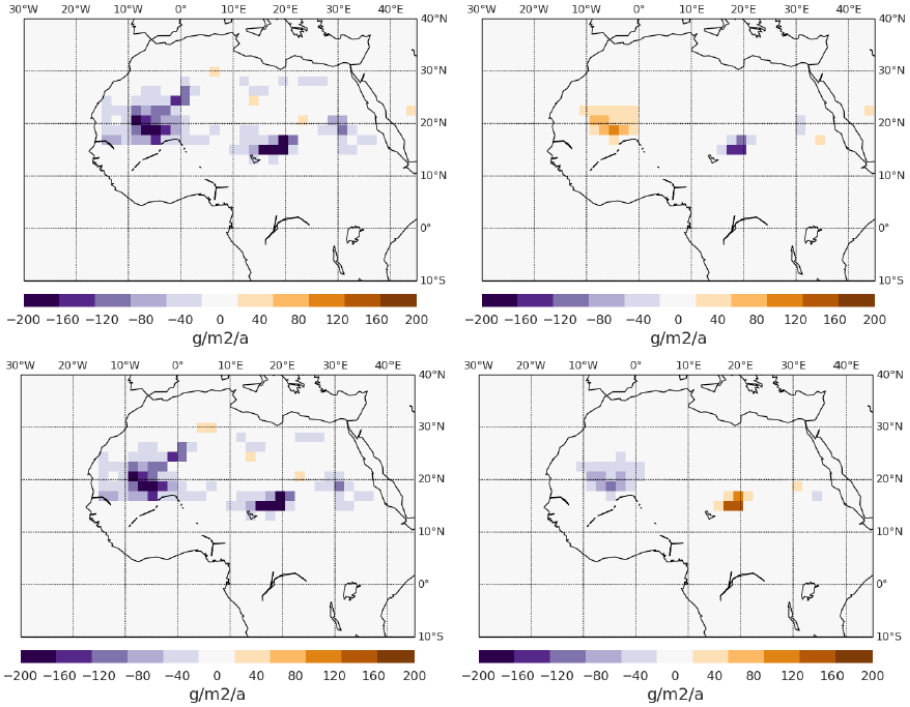

Figure 6. Differences in simulated dust emission in North Africa (17° W–40° E; 10–30° N) between $6k$ and $0k$, Δ_{6k-0k} (top left), Δ_{AO} (top right), Δ_{LV} (bottom left) and the synergy effect Δ_{SYN} (bottom right).

CPD
11, 5269–5306, 2015

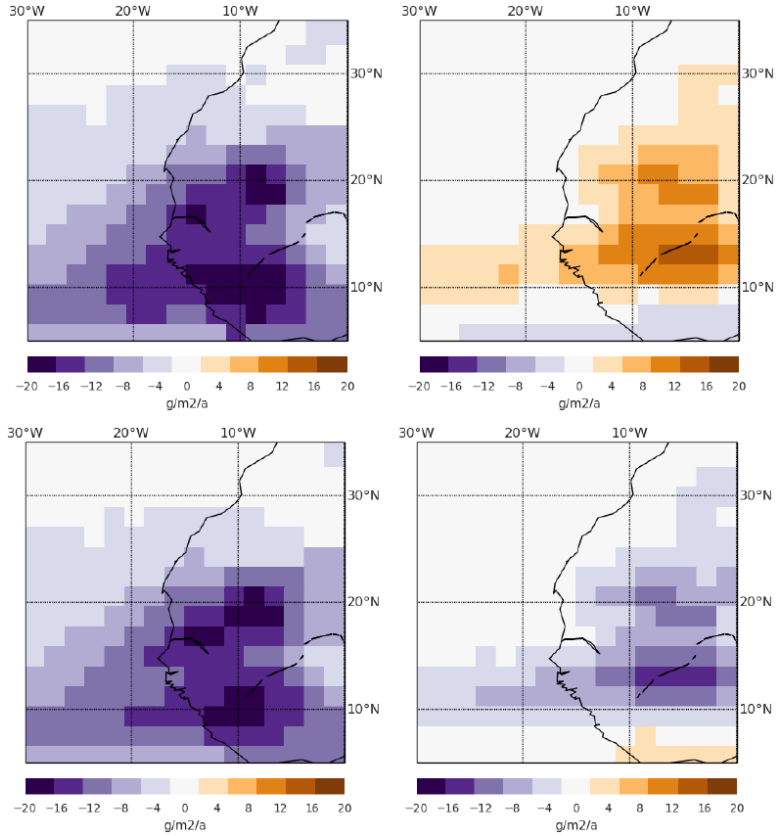

Figure 7. Differences in simulated dust deposition along the northwest African margin (30–17° W; 5–35° N) between 6k and 0k Δ_{6k-0k} (top left), Δ_{AO} (top right), Δ_{LV} (bottom left) and the synergy effect Δ_{SYN} (bottom right).

CPD
11, 5269–5306, 2015

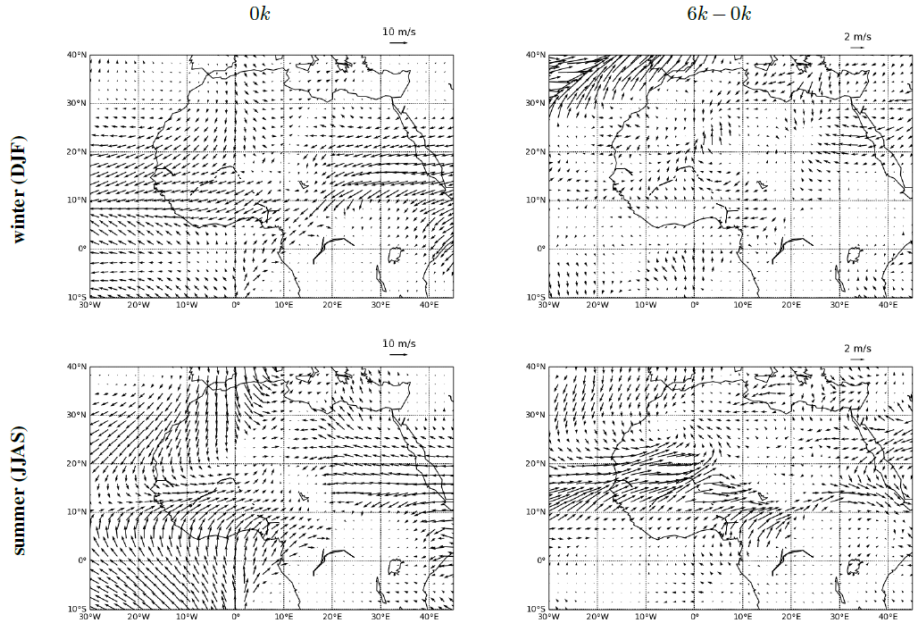

Figure 8. Difference in simulated 10 m surface wind speed and directions for winter (DJF; top) and summer (JJAS; bottom) for 0*k* (left) and for the difference 6*k* – 0*k* (right).

CPD
11, 5269–5306, 2015

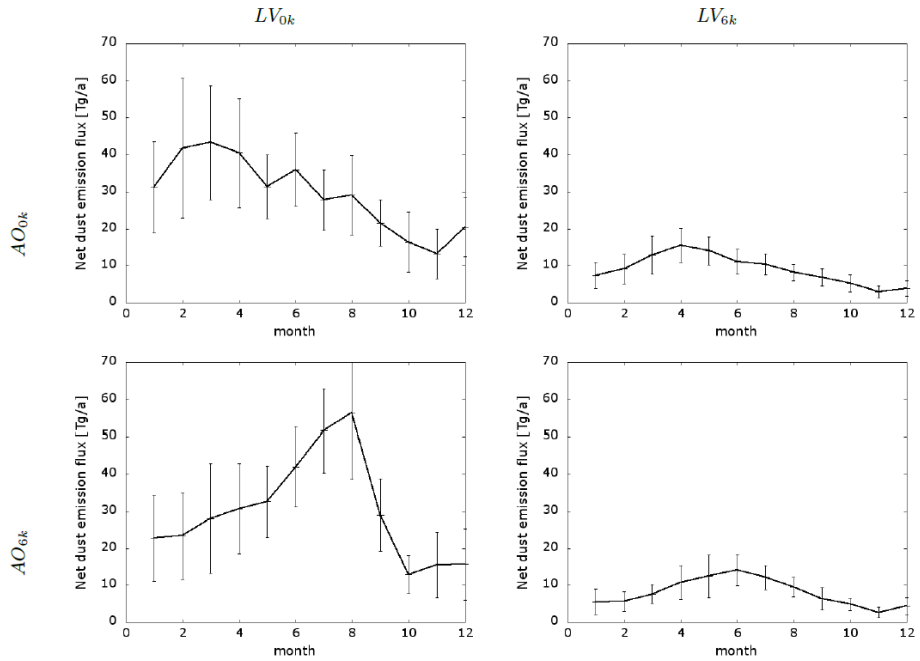

Figure 9. Mean annual cycle of simulated dust emission for altering atmosphere–ocean (AO) and land surface (LV) conditions.

CPD
11, 5269–5306, 2015